Made available through Montana State University's ScholarWorks

Evaluating Cosmic Ray Neutron Sensor Estimates of Snow Water Equivalent in a Prairie Environment Using UAV Lidar

M. Woodley, H. Kim, E. Sproles, J. Eberly, and S. Tuttle

Accessibility Disclaimer:

For a more accessible version of this document, please submit an accessibility request form through the Montana State University Library website.

Check for updates

AGU ADVANCING EARTH AND SPACE SCIENCES

Water Resources Research

RESEARCH ARTICLE
10.1029/2024WR037164

Evaluating Cosmic Ray Neutron Sensor Estimates of Snow Water Equivalent in a Prairie Environment Using UAV Lidar

M. Woodley[1], H. Kim[1], E. Sproles[2,3], J. Eberly[4], and S. Tuttle[1]

[1]Syracuse University, Syracuse, NY, USA, [2]Department of Sciences, Montana State University, Bozeman, MT, USA, [3]Geospatial Core Facility, Montana State University, Bozeman, MT, USA, [4]Central Agricultural Research Center, Montana State University, Bozeman, MT, USA

Abstract Monitoring snow cover in prairie environments is important for understanding water and energy fluxes, agricultural production, and flooding, but difficult due to shallow snowpack and considerable snow heterogeneity. Cosmic ray neutron sensors (CRNS) are sensitive to snow within a radius of 150–250 m, which allows for continuous estimation of snow water equivalent (SWE) over a large footprint and may better represent area-averaged snow cover in prairies than conventional SWE instruments, such as snow pillows. A CRNS was installed at Montana State University's Central Agricultural Research Center (CARC; 47.06°, −109.95°) in Moccasin, MT in coordination with NASA's SnowEx 2021 field campaign. This work assesses the feasibility of a CRNS for SWE monitoring in prairies by comparing CRNS SWE estimates to spatially distributed SWE derived from uninhabited aerial vehicle lidar snow depths within the sensor's footprint and manual snow pit measurements. Lidar observations show snow cover was highly spatially variable, with the largest snow accumulation near barriers and the least in barren fields. Additionally, we evaluate our CRNS SWE estimates using Ultra Rapid Neutron Only Simulation (URANOS) Monte Carlo simulations. Comparisons of SWE estimates derived from lidar, CRNS, and URANOS for shallow snowpack at the site yielded root mean square values of about 2 mm (approximately 30% of the mean SWE). These results suggest that the CRNS is effective at integrating over significant spatial variability within its footprint at this site. However, the spatial distribution of snow exerts a strong influence on the CRNS signal and must be considered when interpreting CRNS observations.

Plain Language Summary Snow in prairie environments can be highly variable due to a lack of tree cover and generally low relief, combined with windy conditions. In this study, we determine how accurately a cosmic ray neutron sensor (CRNS) can estimate snow water equivalent (SWE) for an agricultural site in central Montana. We found that our CRNS was sensitive to changes in the amount of water within a radius of 100–200 m from the instrument. For winter 2020–2021, the site experienced high spatial variability in snow depth, ranging from 1.7 m deep snowdrifts along a major windbreak to shallow snow or bare conditions in the agricultural fields that covered most of our 1 km^2 study site. We compared CRNS SWE estimates at the site to independent SWE estimates derived from lidar snow depth maps and model simulations, and generally found agreement within the uncertainty of each SWE estimation method. This study supports that CRNS can integrate over the significant spatial variability common in prairie snowpacks, but how the snow varies around a given sensor has a strong influence on CRNS SWE estimates and must be considered when interpreting these types of observations.

Key Points:

- We evaluate cosmic ray neutron sensor (CRNS) snow water equivalent (SWE) estimates using spatially distributed snow observations from lidar at a prairie site
- We use neutron transport model simulations to calibrate a site-specific weighting function to represent the spatial sensitivity of a CRNS
- Comparison to model- and lidar-derived SWE show that our CRNS effectively estimates SWE for this heterogenous snowpack

Supporting Information:

Supporting Information may be found in the online version of this article.

Correspondence to:

M. Woodley,
mwoodley@syr.edu

Citation:

Woodley, M., Kim, H., Sproles, E., Eberly, J., & Tuttle, S. (2024). Evaluating cosmic ray neutron sensor estimates of snow water equivalent in a prairie environment using UAV lidar. *Water Resources Research*, *60*, e2024WR037164. https://doi.org/10.1029/2024WR037164

Received 26 JAN 2024
Accepted 5 JUN 2024

Author Contributions:

Conceptualization: S. Tuttle
Data curation: E. Sproles, J. Eberly
Formal analysis: M. Woodley, H. Kim, S. Tuttle
Investigation: M. Woodley, H. Kim, S. Tuttle
Methodology: M. Woodley, H. Kim, S. Tuttle
Resources: E. Sproles
Supervision: S. Tuttle
Validation: M. Woodley, S. Tuttle
Writing – original draft: M. Woodley
Writing – review & editing: M. Woodley, H. Kim, E. Sproles, J. Eberly, S. Tuttle

© 2024. The Authors.
This is an open access article under the terms of the Creative Commons Attribution-NonCommercial-NoDerivs License, which permits use and distribution in any medium, provided the original work is properly cited, the use is non-commercial and no modifications or adaptations are made.

1. Introduction

Northern prairie ecosystems, such as the northern Great Plains of the U.S. and the Canadian prairies, experience cold, dry winters with seasonal snow, frequently frozen soil, and highly variable environmental conditions (Sturm et al., 1995). As one of Earth's most reflective natural surfaces, snow increases land surface albedo and reflects most incoming solar radiation that might otherwise be absorbed by the surface (Hardy et al., 2004; Sturm et al., 2017). Thus, the presence or absence of snow cover in prairies affects regional climate and global energy budgets (Betts et al., 2013). Short vegetation from crop stubble and residual grasses, low relief, shallow snow depths, and snow heterogeneity create a unique environment for snow in prairies (Pomeroy & Li, 2000; Sturm et al., 1995). Crop stubble and residual grasses left over after harvest can also function as a minor windbreak and trap snow. This leads to highly variable, transient snow cover that ranges from deep snow drifts near barriers to

19447973, 2024, 6, Downloaded from https://agupubs.onlinelibrary.wiley.com/doi/10.1029/2024WR037164 by Montana State University Library, Wiley Online Library on [16/08/2024]. See the Terms and Conditions (https://onlinelibrary.wiley.com/terms-and-conditions) on Wiley Online Library for rules of use; OA articles are governed by the applicable Creative Commons License

shallow snowpack to bare, wind-scoured fields that are often redistributed by high winds soon after snow events (Brown & Goodison, 2006; Pomeroy & Li, 2000). This redistribution affects the rate at which the landscape is replenished by melting snow (Lehning, 2006; Shook & Gray, 1997).

Hydroclimatically, a dry atmosphere and high, persistent wind speeds in the prairie increase rate of sublimation and influence ablation rates (Andreadis et al., 2009) thus reducing the residence time of a snowpack. In the prairies, snowpacks often experience repeated snowmelt cycles of melting and freezing that alter percolation rates of water and the amount of water that infiltrates the ground (He et al., 2015). This becomes especially important for agricultural production as the different rates of water infiltration and low snowpack residence times can affect crop water supply and spring planting for agriculture. In Montana, for example, a dominant source of land use is agriculture, with the three of the major crop types grown within the state (i.e., wheat, hay, and barley) accounting for ~$1.8 billion dollars of the state's economy (USDA, 2022). On the other hand, the low relief of prairies can result in a long residence time of water in the drainage network, so relatively moderate snow amounts can lead to significant flooding (Todhunter, 2001). Accurately quantifying the amount of snow in the prairie can help to determine the hydrological impact of snow during springtime. For these reasons, frequent observations of prairie snow are needed to accurately monitor this complex winter environment.

Our study focuses on snow water equivalent (SWE) because it is widely considered the most important snow property for hydrological purposes (Doesken & Robinson, 2009). SWE varies in space and time according to the depth and density of the snowpack (Brown & Goodison, 2006). Traditional ground-based methods for continuous SWE monitoring include snow pillows or snow scales, for example, the SNOTEL network in the western U.S. (Serreze et al., 1999), and snow depth sensors that are paired with snow density estimates from snow models or periodic snow pits to characterize a snowpack (Kim et al., 2017). These instruments are difficult to interpret in prairie snowpacks because of the extreme spatial heterogeneity of snow cover, potentially leading to SWE measurements that are not representative of the areal average. Another disadvantage of snow pillows and snow scales is that they replace the natural ground surface with a smooth, artificial one, which can affect snow accumulation in windy environments like the prairie, while a cosmic ray neutron sensor (CRNS) does not alter the ground surface.

Previous work on above-ground CRNS has documented its utility for estimating SWE (Sigouin & Si, 2016; Wallbank et al., 2021). Sigouin and Si (2016) estimated SWE based on findings from Shook and Gray (1994) that, for shallow snowpacks, SWE follows a linear relationship with snow depth. Sigouin and Si (2016) used manual snow surveys from within the footprint of their cosmic ray sensor and snow precipitation data and found strong agreement between the manual and CRNS SWE estimates. Wallbank et al. (2021) used a network of above-ground and buried CRNS instruments to estimate SWE using the Desilets (2017) method and verified their results from automatic snow depth measurements and a snowmelt model. Some recent work focused on deep snowpacks such as Royer et al. (2021), and Schattan et al. (2017, 2019) found that a CRNS was suitable to monitor deeper alpine snowpacks. This is due to the strong nonlinear correlations between CRNS measurements and SWE derived from Terrestrial Laser Scanning (TLS) surveys.

Our study uses uninhabited aerial vehicle (UAV) lidar snow depth mapping as a primary tool to evaluate CRNS SWE estimates, allowing for high resolution characterization of the spatial snow distribution surrounding the CRNS instrument. We believe our work is the first study to evaluate CRNS SWE estimates using high spatial resolution lidar in a prairie environment. Specifically, our study focuses on the Montana State University (MSU) Central Agricultural Research Center (CARC) in Moccasin, MT, as part of the NASA SnowEx 2021 field campaign. Previous UAV lidar snow depth research has shown that snow depth uncertainty is reported between 1 and 5 cm in open environments (Harder et al., 2020; Jacobs et al., 2021) with higher uncertainty when gaps in lidar data clouds are present. Overall, lidar surveys allow for complete spatial coverage of a CRNS footprint at high spatial resolution and allow for observation of spatial heterogeneity of snow depth within the footprint.

In Sections 2.1 and 2.2 of this manuscript, we introduce the study area and data used in our study, including lidar, in situ snow observations, and CRNS. In Section 2.3, we describe how we obtain CRNS SWE estimates from neutron counts. In Section 2.4, we present Ultra Rapid Neutron Only Simulation (URANOS) neutron transport modeling (Köhli et al., 2023) for the CRNS instrument at the CARC site. In Section 2.5, we describe how we evaluate the CRNS SWE estimates using spatially distributed SWE estimates derived from UAV lidar and ground-based observations. In Section 3, we present the results of our study and analysis, including comparisons between CRNS, lidar, and URANOS-derived SWE estimates. In Section 4, we compare our results to those of

19447973, 2024, 6, Downloaded from https://agupubs.onlinelibrary.wiley.com/doi/10.1029/2024WR037164 by Montana State University Library, Wiley Online Library on [16/08/2024]. See the Terms and Conditions (https://onlinelibrary.wiley.com/terms-and-conditions) on Wiley Online Library for rules of use; OA articles are governed by the applicable Creative Commons License



Figure 1. Study site map. (a) The approximate location of our 1 km^2 study site in Moccasin, MT (indicated by the orange star), including its latitude and longitude in the bottom right corner. (b) An aerial satellite image of the study area (black square) during the summer showing the different agricultural fields. The cosmic ray neutron sensor (CRNS) is in the southwest portion of the study area marked by an orange dot, with an orange circle for its 171 m radius. Three automatic cameras installed near the CRNS are indicated by the numbered yellow stars. Camera 1 is along a large north-south wind break facing west/northwest, where a large snow drift formed. Camera 2 is along the western edge of a field facing east, and Camera 3 is in a wheat field facing east. One snow pit location, Wx, was close to the north end of the snow drift, near Camera 1. The other snow pit location, SnowEx1, is at the south end of the drift near Camera 3 (Basemap image credits: Google, ©08/2016 Landsat/Copernicus).

previous studies, identify the utility and potential limitations of CRNS for prairie snow, and discuss the implications of our study.

2. Materials and Methods

2.1. Study Area

The study area is a 1 km^2 region located in Judith Basin County in central Montana (47.057510°, −109.952945°) containing several agricultural fields managed by the MSU CARC (Figure 1). The study area has very low relief, with elevation ranging from 1,287 to 1,298 m across the study area and a median slope of 0.9° (vertical change of 1.6 cm per meter in the horizontal).

The CARC is an agricultural research site, where researchers investigate different crop varieties, harvest practices, and soil biogeochemistry during the summer months. Crops grown at the site include cereals, grasses, legumes, and broadleaf plants. Harvesting techniques vary and some crops persist into the winter as stubble that can trap snow and affect how readily the snowpack is redistributed by wind (Figure 2). During the winter of 2020–2021, the site had an average air pressure of 870 mbar and an average relative humidity of 62.8%, based on our meteorological measurements. In addition, the air temperature measured by the CRNS averaged −0.4°C during our study period and a DJF average of −3.7°C.

In winter 2020–2021, prairie snow was studied at the MSU CARC as part of NASA's SnowEx field campaign. SnowEx is a multi-year program developed by NASA's Terrestrial Hydrology Program that aims to increase the knowledge and accuracy of snow measurements through airborne and ground observations (Kim et al., 2017; McGrath et al., 2019). For the SnowEx campaign, nine soil profiles with Stevens Water HydraProbe soil moisture and temperature sensors were installed, each with four depths between 5 and 50 cm (Cosh et al., 2022). At each of

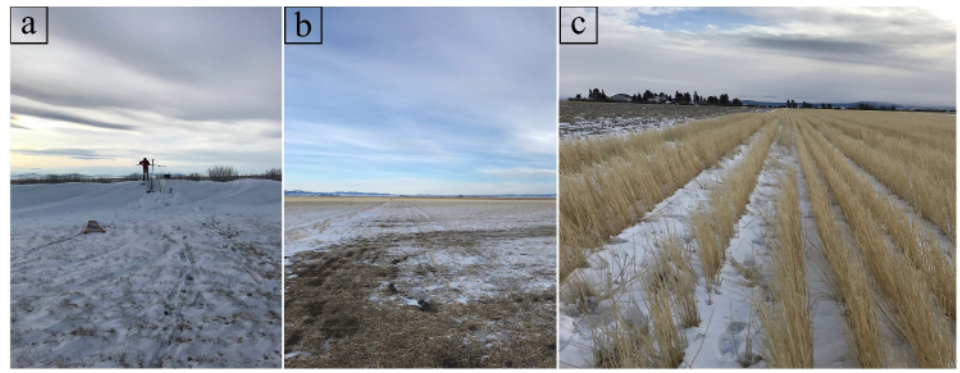


Figure 2. Wind-driven snow in Moccasin, MT creates a pattern of bare fields bordered by deep snow drifts (a and a). Image (a) was taken facing west toward a wind break while image (b) was taken in the same location but facing east toward a bare field. At this part of the study site during mid-February, the snowpack transitioned from a 1.7 m deep snowpack to a nearly absent snow cover within a 30 m distance. Image (c) shows snow captured by crop stubble (Photos: Eric Sproles, 2020–2021 Winter Season).

these sites, a side-looking automated camera and a downward looking infrared radiometer were installed to observe snow depth and snow surface temperature, respectively. The soil moisture probes were distributed across the 1 km^2 study area in fields with various winter cropping practices to analyze varying snow conditions. Three of these sensors were placed near the approximate horizontal footprint of the CRNS (an area with radius of approximately 171 m, based on conventions from previous work (Köhli et al., 2015; Schrön et al., 2017) and our own URANOS modeling results; see Sections 2.4 and 2.5). Additional SnowEx efforts at Moccasin included airborne L-band interferometric synthetic aperture radar flights from the Uninhabited Aerial Vehicle Synthetic Aperture Radar (UAVSAR) instrument, UAV lidar snow depth observations, UAV orthophotos and structure from motion, and ground-based snow observations including snow pits and snow depth transects, some of which were used in this analysis (see Sections 2.2.2 and 2.2.3).

2.2. Data

2.2.1. CRNS

We deployed a CRNS (model CRS2000/B from HydroInnova LLC, Albuquerque, NM, USA) within a spring wheat field at a latitude of 47.059422° and a longitude of −109.955567° (see orange dot in Figure 1) to measure low-energy cosmic ray-induced neutrons. Low-energy neutrons are produced near Earth's surface by the interaction between primary cosmic rays (primarily protons) and nuclei in the atmosphere and attenuated primarily by hydrogen atoms found in soils (Desilets & Zreda, 2001, Figure 1; Zreda et al., 2008). Previous work measuring the cosmic ray neutron count above soils with different saturation levels detailed that the soil moisture content has an inverse relation to the neutron intensity, due to the ability of hydrogen to moderate neutron intensity (Zreda et al., 2008, 2012). Therefore, the fast neutron flux decreases with increasing soil moisture.

The CRNS instrument for this study detects neutrons with energies between 0.2 eV and 100 keV, which allows for the estimation of water in the surrounding area (Desilets et al., 2010; Zreda et al., 2008). We focus our research on neutron counts from the moderated channel of the CRNS, which has been shielded to reduce the number of thermal neutrons and slow epithermal neutrons to detectable energies (Schrön et al., 2018). In snow-free conditions, the CRNS provides an estimate of soil moisture after accounting for water in other parts of the environment, such as atmospheric humidity, water in vegetation, soil organic carbon, and mineral lattice water. If present, snow mass within the CRNS footprint can be estimated by first accounting for soil moisture. To correct atmospheric influences on neutron counts, the CRNS collects air temperature, humidity, and atmospheric pressure data. The instrument collects neutron counts at an hourly rate for a horizontal footprint of approximately 150–250 m and depths of 5–50 cm into the soil, both of which depend on the soil moisture content (Desilets, 2017). From previous work (Köhli et al., 2015) and our own neutron transport modeling (described in Section 2.4) using environmental conditions at the site, we estimate that the footprint radius (i.e., the region within which 86% of the detected neutrons are generated) of our CRNS was approximately 171 m during the study period.

19447973, 2024, 6, Downloaded from https://agupubs.onlinelibrary.wiley.com/doi/10.1029/2024WR037164 by Montana State University Library, Wiley Online Library on [16/08/2024]. See the Terms and Conditions (https://onlinelibrary.wiley.com/terms-and-conditions) on Wiley Online Library for rules of use; OA articles are governed by the applicable Creative Commons License

19447973, 2024, 6, Downloaded from https://agupubs.onlinelibrary.wiley.com/doi/10.1029/2024WR037164 by Montana State University Library, Wiley Online Library on [16/08/2024]. See the Terms and Conditions (https://onlinelibrary.wiley.com/terms-and-conditions) on Wiley Online Library for rules of use; OA articles are governed by the applicable Creative Commons License

Table 1
Uninhabited Aerial Vehicle Lidar Instrumentation Details

Instrument	Wavelength (nm)	Equipment	Use	Dates
Phoenix Lidar Systems Ranger LR	1,550	Northrup Grumman LN200C Fiber Optic Gyroscope (FOG) IMU	"Snow-off" flight; DTM	15 January
		Novatel OEM 617 GNSS receiver		
		Novatel Pinwheel GNSS antenna		
Phoenix Lidar Systems miniRanger	905	Inertial Labs IMU-P IMU	"Snow-on" flights; DSMs	21, 22, and 29 January
		Novatel OEM 7720 GNSS receiver		17, 18, and 24 February
		Novatel Pinwheel GNSS antenna		4 March

Direct measurements of soil moisture during snow-free conditions are necessary to calibrate CRNS neutron counts to the amount of water in the surrounding environment. Soil samples were collected on 6 May 2021, at which time the site was snow-free. The samples were collected in a radial pattern at three distances in each of six directions from the instrument, for a total of 18 locations, with six samples from each location (5 cm intervals from 0 to 30 cm depth), following the protocol from Zreda et al. (2012). The soil samples were weighed and then dried at −60°C for 3 days and reweighed to obtain gravimetric soil moisture (Cosh et al., 2022). Twenty-six of the 108 samples (24%) were not recoverable due to poor soil coherence. Prior to averaging, we estimated missing soil moisture values using a multiple regression model. This model was fitted to the existing soil moisture data, with depth and soil profile location as independent variables, and soil moisture values for the missing soil samples were predicted using the fitted regression. We attempted to mitigate any bias in the areal average soil moisture due to a higher or lower number of missing values for any given depth, distance, or direction. Additionally, composite soil samples were analyzed by Activation Laboratories Ltd. (Ancaster, Ontario, Canada) to determine the soil organic carbon content and the amount of water in the soil mineral lattice at the site.

2.2.2. Lidar

Lidar data for the 1 km^2 study area were acquired by a private contractor, DJ&A, P.C., via UAV flights for one "snow-off" date and seven "snow-on" dates. The "snow-off" flight refers to the first day of collection, 15 January 2021. On this date, most of the site was snow-free, except for a snow drift on the leeward eastern side of a north-south wind break in the western portion of the study area (see Figure 2). Snow-on flights refer to days with more extensive snow cover later in winter 2021. Information about the UAV-mounted lidar instruments used for the UAV flights are shown in Table 1. Note that DJ&A switched to a 905 nm wavelength laser for the "snow-on" flights because it has better reflectance for snow and ice conditions (Deems et al., 2013), which was reaffirmed with their own field tests.

At least 28 RTK Global Navigation Satellite System (GNSS) points from Trimble R10 GNSS base stations and rovers were collected for each lidar acquisition date and used to for ground truthing the lidar data. For ground truth points on snow surfaces, DJ&A used a GNSS rover mounted on a survey rod and equipped with a laser distance meter to obtain accurate height measurements for each RTK shot. These heights were periodically verified using a tape measure, with agreements of 2 mm or less. Additional GNSS points were collected for six triangular plates on tripods placed throughout the study area and used for additional quality control. The truthing points were used for assessment of global and absolute accuracy of the lidar point clouds.

For all snow-on conditions during the study period, ground truthing showed that the true snow surface was near the top of the lidar clouds for the 905 nm lidar used for the "snow-on" flights, not in the middle of the point cloud as was expected and observed for bare ground. DJ&A therefore used a custom iterative ground classification approach and manually reviewed the resulting ground classes to identify the snow surface from the lidar point clouds. The point clouds for each lidar acquisition were then aligned with the point cloud for the "snow-off" acquisition using a uniform vertical shift value that was unique to each acquisition date. This vertical shift value was determined by comparing each "snow-on" point cloud to the "snow-off" point cloud in areas where they should align, such as cleared parking lots and train tracks. This process allowed the point clouds to remain aligned with each other, while also allowing for acceptable vertical accuracy. From the aligned lidar point clouds, DJ&A generated digital models of surface elevation at 30 cm spatial resolution for each UAV flight. This included two

versions of a "snow-off" digital terrain model (DTM), with surface elevation of the snow drift included and omitted, respectively, and seven "snow-on" digital snow models (DSM; surface elevation generated using lidar data from a date with snow cover). These DTM and DSMs were used in our analysis.

2.2.3. Other Ground-Based Snow Observations

We also used ground-based observations to evaluate our CRNS SWE estimates. These included side-looking automatic cameras for snow depth and manual ground-based snow observations. The automated camera images allowed us to observe field conditions, especially the snow cover distribution. WingScapes TimelapseCam Pro cameras mounted on U-posts collected images every hour from 07:00 to 17:00 local time each day from November 2020 until 2 April 2021, when they were removed for spring planting. Each camera had a painted stake that could be used to infer snow depth within its view. Three cameras were placed within or near the footprint of the CRNS (see Figure 1) to provide daily snow cover conditions.

Manual snow measurements used in this analysis were from two snow pit locations: Wx (northern portion of the snow drift) and SnowEx1 (southern portion of the drift) that included profiles of snow temperature, density, and grain characteristics, as well as field conditions during site visits (see Figure S2 and Text S2 in Supporting Information S1). These snow pit observations were collected on 20 January, 17 February, 24 February, and 5 March, which coincided with four of the lidar flights (except 21 January lidar flight that occurred one day after 20 January snow pits due to windy conditions, and 4 March lidar flight that occurred one day before 5 March snow pits).

2.3. CRNS SWE

We estimated SWE for the CRNS based on the attenuation of low-energy neutrons beyond a baseline soil moisture, where the neutron counts were calibrated to measured soil moisture at our site (Desilets, 2017; Desilets et al., 2010; Schrön et al., 2017; Zreda et al., 2012). After correcting the neutron counts for solar activity, atmospheric pressure, and humidity (Desilets, 2017; Rosolem et al., 2013), SWE was estimated from the moderated channel of the CRNS using Equation 1 (Desilets, 2017).

$$\mathrm{SWE} = -\Lambda \ln \frac{(N - N_{\mathrm{wat}})}{(N_{\mathrm{init}} - N_{\mathrm{wat}})} \tag{1}$$

N is the counting rate of the moderated neutrons measured by the instrument, after the above-mentioned corrections. N_{wat} is the counting rate over an infinite depth of water, and N_{init} is the counting rate of the CRNS moderated channel over bare soil immediately prior to the first snowfall. Desilets et al. (2010) used neutron transport models to find an attenuation length (Λ) of 4.8 cm. N_{wat} is calculated by the following equation:

$$N_{\mathrm{wat}} = 0.24 N_0, \tag{2}$$

where 0.24 is an assigned constant value (Desilets, 2017; Desilets et al., 2010). N_0 is the theoretical counting rate of the neutrons over dry soil:

$$N_0 = \frac{F(t) N_\theta}{\frac{a_0}{\theta_g + a_2} + a_1}, \tag{3}$$

where $F(t)$ is the total neutron count correction factor from solar activity, atmospheric pressure, and humidity, $a_0 = 0.0808$, $a_1 = 0.3720$, and $a_2 = 0.1150$ (Desilets, 2017; Desilets et al., 2010). θ_g is gravimetric water equivalent (i.e., the sum of soil moisture, soil mineral lattice water (Dong et al., 2014), and water equivalent of soil organic carbon (Hawdon et al., 2014)) from in situ soil samples and N_θ is the neutron counting rate at the time of the gravimetric sampling. To find N_0, we used the updated "revised" vertical and horizontal weighting scheme from Schrön et al. (2017). We calculated the averaged gravimetric water content (θ_g) by vertically and horizontally weighing the soil samples collected on 6 May 2021 (see Section 2.2.1). From the final averaged soil water equivalent, we compared and calibrated it to our CRNS product to derive the calibrated N_0 (Schrön et al., 2017).

For CRNS SWE estimation, we applied our calibrated N_0 to Equations 1 and 2. Unfortunately, there was no period where the study area was completely snow-free between the installation of the CRNS on 22 November 2020 and

19447973, 2024, 6, Downloaded from https://agupubs.onlinelibrary.wiley.com/doi/10.1029/2024WR037164 by Montana State University Library, Wiley Online Library on [16/08/2024]. See the Terms and Conditions (https://onlinelibrary.wiley.com/terms-and-conditions) on Wiley Online Library for rules of use; OA articles are governed by the applicable Creative Commons License

the "snow-off" lidar flight on 15 January 2021. Because the soil moisture calibration for the CRNS occurred after the winter season due to the lack of snow-free conditions after CRNS installation, we chose the "snow-off" lidar flight on 15 January 2021, when only a small portion of the study area was snow covered and we were able to estimate that small snow amount using lidar, to serve as the baseline condition for N_{init} in Equation 1. We averaged the neutron counts from 9 a.m. to 5 p.m. MST on 15 January 2021, as N_{init}. Thus, all CRNS, lidar, and model SWE estimates in this study are differences in the amount of SWE relative to 15 January 2021.

2.4. Neutron Transport Modeling

2.4.1. Ultra Rapid Neutron Only Simulation (URANOS)

We used neutron transport modeling to generate a spatial sensitivity function for the CRNS, and as an additional source of evaluation for CRNS SWE estimates. We used a freely available neutron transport model, the URANOS v1.14 (Köhli et al., 2015, 2023, available at https://gitlab.com/mkoehli/uranos), to model the neutron flux under conditions observed at our study area. URANOS utilizes a Monte Carlo approach to simulate the neutrons and has been specifically developed for CRNS applications (Köhli et al., 2023), including monitoring soil moisture changes through irrigation (Brogi et al., 2022) and monitoring SWE (Schattan et al., 2019). In URANOS, millions of neutrons are generated from randomly distributed point sources within a user-defined area, while tracking each neutrons' paths and interactions from its source to the point of detection through a ray casting algorithm (Köhli et al., 2023). URANOS can model 3-dimensional voxel-based geometries with defined materials by stacking multiple layers of either ASCII matrices or bitmap images to replicate important site characteristics (Köhli et al., 2023).

2.4.2. Model Domain and Neutron Transport Simulations

We executed eight simulations in URANOS that correspond with 15 January "snow-off" and seven subsequent "snow-on" lidar flights. The spatial distribution of SWE used to initialize each simulation was determined from the UAV lidar observations and snow density estimates on the given date. We used 15 January as the control, and lidar-derived SWE from the seven "snow-on" flights for the remaining simulations. We used the neutron counts output from the model simulations to estimate SWE and compared those model estimates to CRNS and lidar-derived SWE. We also executed a "no snow" model simulation, where the neutron transport was determined only by soil and atmospheric conditions, to derive the site-specific spatial weighting function for the CRNS (Section 2.5).

The geometries used for URANOS simulations and the approximate footprint of the CRNS are shown below in Figure 3. The neutrons in the simulations were generated in the source layer, a 30 m thick layer placed 50 m above the ground (Köhli et al., 2023). The neutron generating area (dashed circle, Figure 3) was set to a circular shape with a radius of 707 m in our source layer to completely cover our research domain (blue square, Figure 3). The URANOS simulator generates and propagates the neutrons lower in the atmosphere to save computation resources (Köhli et al., 2023). The detector layer, located approximately 2 m above ground, defines where the neutron detector is located (Köhli et al., 2023). While the entire layer can be used as a detector, we simulated a real CRNS instrument in URANOS as an absorbing 9 m radius vertical cylinder with simulated detector efficiency (see below), placed at the location of the CRNS instrument within the 1 km^2 study region. Using an enlarged virtual detector, as opposed to its actual dimension, is standard in URANOS for the purpose of saving computational time and gathering more detection statistics (Köhli et al., 2023). The virtual detector in URANOS had the same characteristics as a CRNS instrument, in that the simulated detector removed the neutrons from the simulation after detection (Köhli et al., 2023).

Our model domain was the 1 km^2 area with a 2 m spatial resolution, as shown in Figure 3. To generate snow layers, we resampled the lidar snow depth DSMs to 2 m resolution, due to model specifications. As mentioned in Section 2.4.1, we can define a 3-dimensional geometry by stacking either a bitmap image or ASCII text file which is limited to 500 by 500 pixels. To cover our entire study region, we resampled our measurements to fit a 500 by 500 ASCII array. In URANOS, we added a 500 m buffer zone on top of our 1 km by 1 km research domain. Any neutrons that traveled outside of this buffer zone were removed from the simulation. Snow layers were split at semi-regular intervals, with thinner layers close to the ground, defined at 0–1 cm, 1–2.5 cm, 2.5–5 cm, 5–10 cm, 10–20 cm, and then every 20 cm until the maximum snow depth. Snow density layers were similarly created for each layer based on the two-layer density scheme adopted for the lidar-derived SWE.

19447973, 2024, 6, Downloaded from https://agupubs.onlinelibrary.wiley.com/doi/10.1029/2024WR037164 by Montana State University Library, Wiley Online Library on [16/08/2024]. See the Terms and Conditions (https://onlinelibrary.wiley.com/terms-and-conditions) on Wiley Online Library for rules of use; OA articles are governed by the applicable Creative Commons License

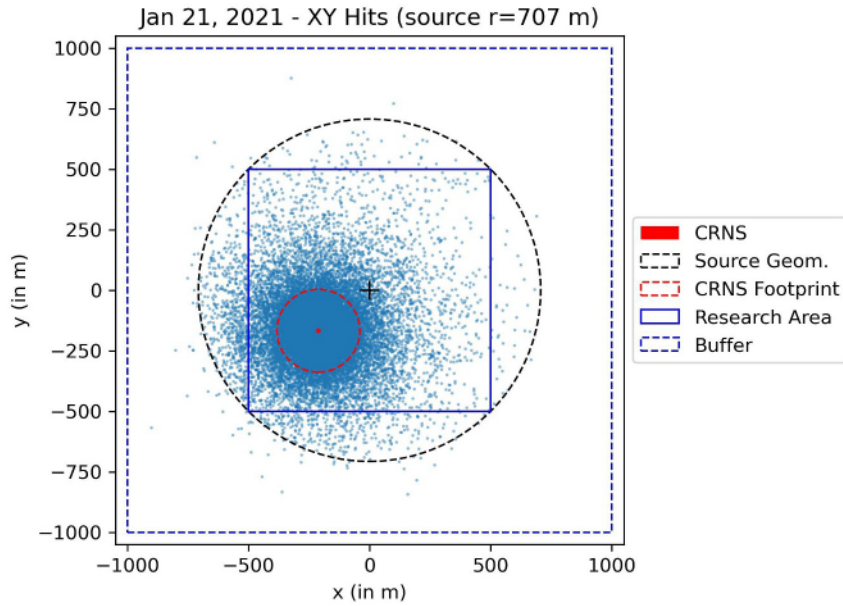


Figure 3. Example map showing neutron hits (blue dots) from the Ultra Rapid Neutron Only Simulation (URANOS) output for 21 January 2021 "snow on" date. The 1 km^2 study region of the CARC (Figure 1) is shown in the solid blue box. The black dashed line shows the URANOS neutron source geometry, a circle with radius of 707 m to cover the entire study region. The red dot shows the location of the simulated cosmic ray neutron sensor (CRNS) detector. The red dashed circle shows the CRNS footprint, calculated to be approximately 171 m based on a spatial weighting function calibrated to URANOS outputs (see Section 2.5). A 500 m boundary zone outside of the 1 km^2 study region (dashed blue box) was set to remove any neutrons from the simulation that passed this threshold.

Within URANOS, the soil layers were separated from the overlying snow layers by defining a distinct ground layer (Köhli et al., 2023). Maps of soil moisture, porosity, and bulk density were generated through interpolation using inverse distance weighting of the in-situ soil measurements described in Section 2.2.1. Each individual 5 cm soil layer was stacked to model the soil moisture conditions from 6 May 2021 soil samples, and kept constant across all model simulations. A final 1.3 m soil layer (1% soil water content at 50% porosity) was added below the top 30 cm of soil layers to increase the total soil depth to 1.6 m. Similarly, atmospheric density and humidity were kept constant using 15 January values (888 mbar and 3.341 g m^{-3}, respectively) across all simulations to reduce the number of influencing variables on neutron flux. This approach followed previously published research and justified by the corrections applied to CRNS measurements due to barometric pressure and atmospheric humidity as mentioned in Section 2.3 (Schattan et al., 2019). Constant atmospheric and soil moisture conditions in the model allowed us to compare changes in neutron count due to the changing snow distribution on the different lidar dates.

Despite the large number of neutrons that are generated in a typical URANOS run (10^7 to 10^9), only a small fraction intersect the simulated detector (Köhli et al., 2023). For neutrons that intersect the detector, the probability of detection is dependent on both neutron parameters (e.g., energy and direction) and sensor parameters (e.g., geometry and moderator type) (Köhli et al., 2023). To create a realistic simulation of a CRNS probe in URANOS, we specify a detector response function (DRF). We utilized a DRF with a high-density polyethylene moderator of 25 mm thickness, consistent with the properties of the actual moderated detector of our CRNS instrument (Köhli et al., 2018). The DRFs were provided through ASCII-files containing energies and weights and are readily available at the URANOS GitLab repository (https://gitlab.com/mkoehli/uranos). To calculate the neutron counts from the model outputs, we applied a method from Brogi et al. (2022) to interpolate the DRF for the 25 mm thick H P D E (HPDE) with a cubic spline to create a continuous curve. We assigned a weight to each simulated neutron depending on the energy during detection, and then summed to obtain the total neutron count (Brogi et al., 2022).

We calculated SWE from our model outputs using Equation 1 and the DRF-filtered neutron counts, calibrated from the near snow-free conditions of 15 January. We held our calibration values constant in Equations 1–3 using

19447973, 2024, 6, Downloaded from https://agupubs.onlinelibrary.wiley.com/doi/10.1029/2024WR037164 by Montana State University Library, Wiley Online Library on [16/08/2024]. See the Terms and Conditions (https://onlinelibrary.wiley.com/terms-and-conditions) on Wiley Online Library for rules of use; OA articles are governed by the applicable Creative Commons License

19447973, 2024, 6, Downloaded from https://agupubs.onlinelibrary.wiley.com/doi/10.1029/2024WR037164 by Montana State University Library, Wiley Online Library on [16/08/2024]. See the Terms and Conditions (https://onlinelibrary.wiley.com/terms-and-conditions) on Wiley Online Library for rules of use; OA articles are governed by the applicable Creative Commons License

15 January as the neutron count baseline (i.e., source of N_{init}, θ_g, and N_θ). SWE was estimated for the corresponding "snow-on" dates by comparing the changes in neutron counts relative to 15 January model simulation. The URANOS simulated SWE values were compared to CRNS SWE estimates.

2.5. Evaluation of CRNS SWE

We compare hourly and daily averaged SWE derived from our CRNS neutron counts to several instruments installed at the CARC site to evaluate whether the CRNS SWE estimates are accurate and representative of this prairie region. Soil moisture sensors installed at the CARC, three of which were within or near the 171 m horizontal footprint of the CRNS, are not used in this analysis. The soil moisture sensor data effectively become unusable from early November until mid-March, when the temperature measurements from the probes dropped below 4°C. Below that point, dielectric effects during the phase change from liquid water to ice complicates interpretation of the soil moisture data. The soil column down to 50 cm remained below 4°C from early November until late March, with the top 10 cm at or within 1°C of freezing for the entire period. Instead, we used the TimelapseCam Pro cameras to confirm presence of snow on the ground and whether those periods match changes in CRNS SWE after known snow events and further supported by field observations during site visits.

Lidar snow depth maps were calculated by subtracting the "snow off" DTM from the "snow on" DSM for a given date, with the difference representing the snow depth on that date. Because some limited areas of snow were present on the date of the "snow off" UAV flight on 15 January 2021 (to the east of the north-south windbreak where a persistent snow drift formed), DJ&A provided a DTM with the snow-covered areas masked out. To estimate the land surface elevation in the masked area near the snow drift, we gap-filled the DTM using universal kriging spatial interpolation with a Bessel variogram model prior to subtraction from the DSMs. We assigned a snow depth of 0 to any lidar snow depth pixel with a negative value, as these likely resulted from error in generating or aligning the lidar point clouds, or the influence of crop stubble. Throughout the winter, most of the CRNS footprint was covered by shallow snow, while a small portion of the western side of the footprint included the deep snowdrift.

On two dates, 22 January and 24 February, lidar snow depth observations did not encompass the entire 1 km^2 study area (88% and 87%, respectively) due to adverse winter conditions. The missing areas were from the eastern and western portion of the study area, respectively. The missing lidar observations did not extend into the 171 m radius CRNS footprint on 22 January, and only 1.4% of the footprint was missing on 24 February. To avoid biasing the SWE from these dates by spatially weighing over an incomplete lidar-derived SWE map, we gap-filled the missing portion of the footprint using multiple linear regression. The dependent variable in the regression was the lidar snow depth data within the CRNS footprint on the given date, omitting the missing portion, and the independent variables were the lidar snow depth from all other dates, also omitting the same missing portion of the footprint. Each date with lidar snow depth was a different independent variable, and each pixel was an observation within those variables. This preserved some information about how the snow depth on each date related to the magnitude and distribution on the date of interest. The regression was then used to gap-fill the missing portion of the 1 km^2 study area. While we do not expect that these predictions perfectly reproduced the distribution of snow in the missing portion of the footprint, it was likely sufficient to reduce bias when calculating spatially averaged SWE over the CRNS footprint, or for inputs to neutron model simulations.

To calculate SWE from lidar snow depth maps, snow density is required. Limited snow density measurements (two snow pits within the CRNS footprint on each of four dates, and only within the snow drift) are available, so it was necessary to make assumptions about the spatial distribution of snow density within the study area. Snow pit data revealed that the base of the snow drift consisted of very dense snow (approximately 400–500 kg/m^3), often overlain by lower density snow, with the two separated by melt-refreeze layers. Snow in the less dense, upper portion of the snow pits ranged from approximately 100 kg/m^3 for newly fallen snow to slightly over 400 kg/m^3 late in the melt season. Qualitative field observations consistently indicated that the shallow snow covering most of the study area was of lower density than the base of the deep snow drift. Therefore, we adopted a two-layer density scheme based on snow density measurements from the snow pits to estimate distributed snow density throughout the study area, with an upper less dense layer atop a persistent, denser basal layer. Distributed maps of the depth of the lower density, upper snow layer were obtained by subtracting the snow depth between subsequent lidar flights that occurred before and after snow events (see Text S2 in Supporting Information S1 for details). In the case where both less dense and more dense snow layers existed, SWE contained in the "light" and "dense"

19447973, 2024, 6, Downloaded from https://agupubs.onlinelibrary.wiley.com/doi/10.1029/2024WR037164 by Montana State University Library, Wiley Online Library on [16/08/2024]. See the Terms and Conditions (https://onlinelibrary.wiley.com/terms-and-conditions) on Wiley Online Library for rules of use; OA articles are governed by the applicable Creative Commons License

layers were calculated separately, and then summed to find the total SWE for the given lidar pixel. SWE was determined for each of the two snow layers for each lidar pixel (SWE_{lidar}) by dividing the density of the given layer estimated from the snow pit measurements (D_{snow}) by the density of water, D_{water}, and multiplying by the depth of the given snow layer (Equation 4).

$$SWE_{lidar} = SD \times \frac{D_{snow}}{D_{water}} \tag{4}$$

The sensitivity of an aboveground CRNS to its surrounding area is not constant with distance; more of the neutrons that reach the detector originate near the instrument, rather than far away. Thus, to compare gridded lidar-derived SWE to the CRNS SWE, we spatially averaged the lidar-derived SWE in a way that approximates the CRNS sensitivity as a function of distance from the detector. While previous neutron modeling studies indicated that the CRNS sensitivity decreases approximately exponentially with distance (Andreasen et al., 2020; Desilets, 2017; Desilets & Zreda, 2013), more recent studies indicate that CRNS are much more sensitive to the area immediately surrounding the instrument than an exponential function and decreases somewhat more linearly with distance (Köhli et al., 2015; Schrön et al., 2017). Schrön et al. (2017) defined a spatial weighting function for aboveground CRNS as a function of air pressure, atmospheric humidity, soil moisture, and vegetation. However, we found that the Schrön et al. (2017) weighting function was a decent but imperfect fit to the distribution of neutron density as a function of distance from the detector in our neutron transport model simulations (see Section 2.4). So, we derived our own spatial weighting function by fitting a multi-exponential equation (like the formulation in Schrön et al., 2017) to the distribution of neutron density from our "no snow" neutron transport model simulation using nonlinear least squares. This yielded a spatial weighting function defined as:

$$W(r) = \left(6{,}684.67 \cdot e^{\frac{r}{1.6}} + 171.821 \cdot e^{\frac{r}{16.315}} + 154.926 \cdot e^{\frac{r}{116.94}}\right) \cdot \left(1 - e^{(-3.7 \cdot r)}\right) \tag{5}$$

In Equation 5, $W(r)$ is the value of the spatial weighting function as a function of distance (m) from the CRNS detector, r. The CRNS footprint is defined as a radius within which 86% of the detected neutrons originate, which corresponds to 171 m for Equation 5. Because the spatial weighting function was derived from URANOS simulations without a snow layer, this weighting function is independent of lidar snow depth.

To apply our custom multiexponential weighting function to a gridded data set of SWE (or soil moisture), the weight for each given pixel can be calculated as:

$$W_{pixel}(r) = \frac{W(r)}{2 \cdot \pi \cdot r} \cdot A_{pixel} \tag{6}$$

where $W_{pixel}(r)$ is the weight to assign to a given pixel, $W(r)$ is the custom multiexponential function from Equation 5, r is the distance from the center of the pixel to the CRNS detector, and A_{pixel} is the pixel area. In our case, the lidar data are gridded to 30 cm resolution, so A_{pixel} is equal to 0.09 m^2.

To calculate the spatially weighted lidar-derived SWE, we multiply the weight for each pixel by the SWE value for that pixel, and sum the product for all n pixels, and then divided by the sum of the weights for all pixels.

$$SWE_{lidar} = \frac{\sum_{i=1}^{n} SWE_{pixel} \cdot W_{pixel}(r)}{\sum_{i=1}^{n} W_{pixel}(r)} \tag{7}$$

For this weighted averaging, we restrict the lidar data to a 300 m radius surrounding the CRNS (equivalent to approximately 95.3% of the total weighting function) due to the CRNS proximity to the boundary of the study area and correct the estimated SWE for the remaining 4.7% of the total weight that is outside of the 300 m radius.

For comparison of lidar-derived SWE and CRNS SWE estimates, we fitted a simple linear regression and calculated the coefficient of determination (R^2). In addition, the root mean squared error (RMSE), mean bias error (MBE), and mean absolute error (MAE) were calculated for comparisons between lidar-derived SWE, CRNS SWE, and modeled SWE.

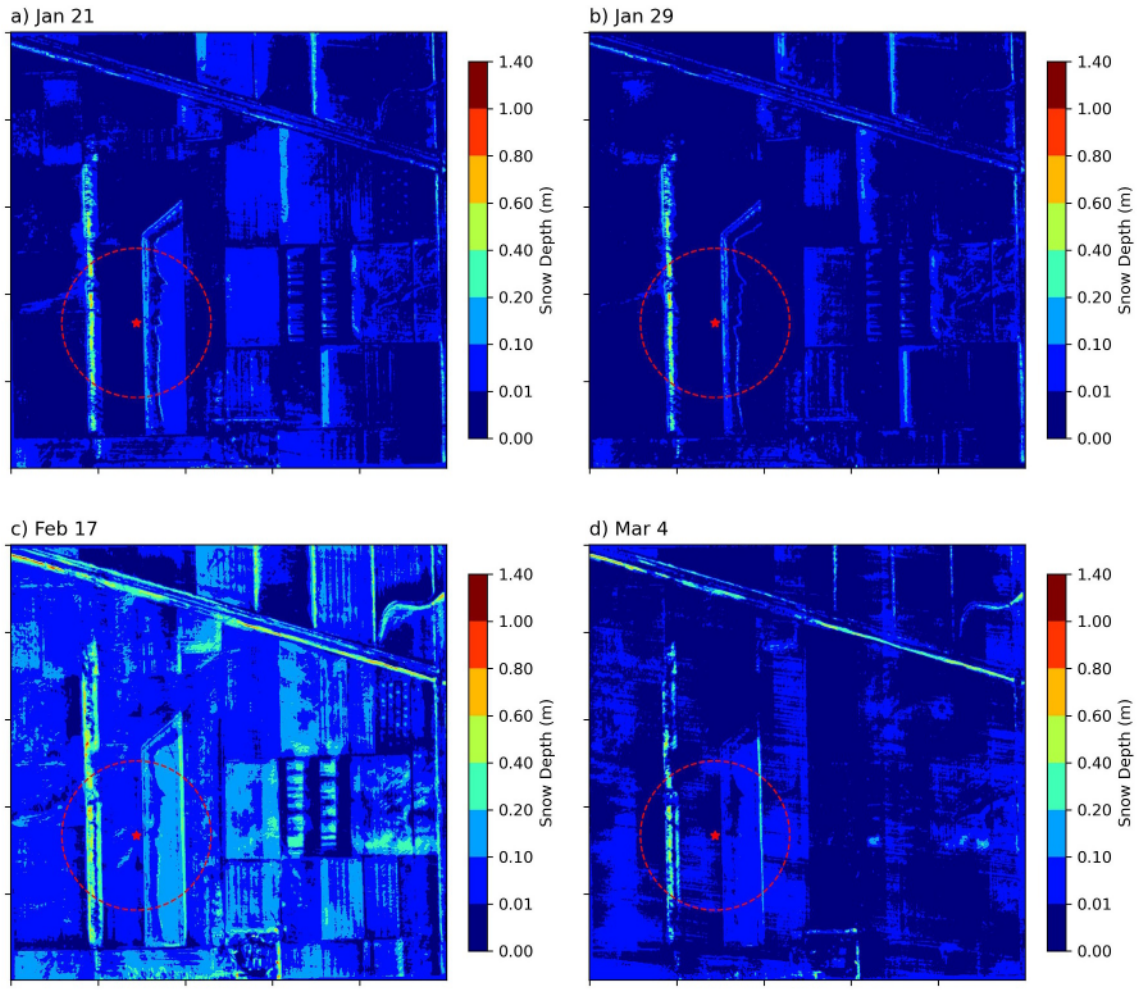


Figure 4. Snow depth maps derived from UAV-based lidar for four example dates in Moccasin, MT during SnowEx 2021 campaign. Each snow map represents the difference in surface elevation in meters from a digital snow model (DSM) compared to a snow-free digital terrain model (DTM). The approximate location of our cosmic ray neutron sensor instrument is marked on each map by a red star, with a red circle representing its 171 m radius footprint.

3. Results

At the CARC study site in Moccasin, MT, the snowpack was highly variable in space, but showed consistent patterns of accumulation over time. During mid-winter, the snow transitioned from up to 1.7 m deep snow drifts along a north-south wind break (Figure 4, western portion of the study area) to bare fields within a 30 m distance (e.g., Figures 2a and 2b). This rapid shift in snow depth over a small distance illustrates the potential for considerable snow variability in the prairie. Lidar snow depth maps (Figure 4) from winter 2020–2021 show that the largest snow accumulation occurred along barriers, especially east of the north-south wind break. Additional snow drifts formed during the later winter months along boundaries between the different crop fields, along the railroad that runs WNW—ESE across the northern portion of the study area, and in areas where crop stubble was present (e.g., see Figure 2c).

Spatial average snow depths and SWE at the site were low, with values ranging from 1.0 to 7.9 cm and 0.03 to 0.11 cm for observed snow depth and estimated SWE, respectively. The largest snow depths detected by lidar occurred on 17 February (as seen in Figure 4) and 18 February. During each lidar "snow-on" day, the lidar contractors measured a vertical RMSE or uncertainty in the lidar snow depths. For the corresponding days of 21 January, 22 January, 29 January, 17 February, 18 February, 24 February, and 4 March, the contractors DJ&A reported vertical DSM uncertainties of 6.8, 7.7, 7.6, 7.9, 9.2, 6.3, and 3.9 cm, respectively. Other work at this site performed by Palomaki and Sproles (2023) comparing the DJ&A lidar from 21 January to point observations from

19447973, 2024, 6, Downloaded from https://agupubs.onlinelibrary.wiley.com/doi/10.1029/2024WR037164 by Montana State University Library, Wiley Online Library on [16/08/2024]. See the Terms and Conditions (https://onlinelibrary.wiley.com/terms-and-conditions) on Wiley Online Library for rules of use; OA articles are governed by the applicable Creative Commons License

19447973, 2024, 6, Downloaded from https://agupubs.onlinelibrary.wiley.com/doi/10.1029/2024WR037164 by Montana State University Library, Wiley Online Library on [16/08/2024]. See the Terms and Conditions (https://onlinelibrary.wiley.com/terms-and-conditions) on Wiley Online Library for rules of use; OA articles are governed by the applicable Creative Commons License

20 January showed uncertainties on the range of approximately 20 cm, higher than any reported in the DJ&A report. However, this uncertainty was calculated from manual snow depth observations on different, consecutive days, because the lidar flights had to be postponed due to strong winds. We believe snow redistribution occurred during the intervening period, resulting in the larger estimated lidar uncertainty found in Palomaki and Sproles (2023).

A time series of the corrected neutron counts from the moderated channel of the CRNS for winter 2020–2021 (see Section 2.3) is shown in Figure 5b. CRNS SWE derived from these neutron counts is shown in Figure 5a. The neutron counts have an inverse relationship with the SWE estimates; when there is more hydrogen (i.e., water) present in the surrounding area, the counts decrease. The CRNS SWE data increase concurrently with snow events (Figure S1 in Supporting Information S1), which were observed during site visits and are evident in the lidar snow depth maps (Figure 4). Additionally, the highest peaks in CRNS SWE closely match the lidar snow depth maps with the deepest snowpack (17 February, 18 February, and 24 February), which were taken within days of major snowstorms. The snow events observed in lidar snow depth and CRNS SWE are further substantiated by three snow stake cameras within or near the CRNS horizontal footprint (see Figure 1b), also shown in Figure S1 in Supporting Information S1.

Comparison of CRNS SWE estimates versus the corresponding spatially weighted lidar snow depth from the 7 days of lidar collection showed a high positive correlation with a Pearson's r of 0.97 and a Spearman's ρ of 0.93. This agreement suggests that the CRNS is sensitive to snow amount. However, SWE versus snow depth is not a direct comparison as snow density can vary significantly in shallow snowpacks. To test the accuracy of the averaged CRNS SWE estimates, we compared CRNS SWE (see Section 2.3) to independent SWE estimates derived from lidar snow depth and snow density from the snow pits (see Section 2.5), as well as SWE estimates from URANOS model simulations (see Section 2.4).

Figure 6 shows the comparisons between the SWE estimates from the CRNS and lidar observations, and URANOS simulations (see Section 2.4). Spatially weighted average lidar SWE RMSE values were calculated from Monte Carlo simulations by adding random error to the lidar snow depth maps based on the reported vertical uncertainty of the lidar measurements and propagating the snow depth plus added error through the snow density and spatial weighting calculations to obtain SWE uncertainty. CRNS and model SWE uncertainties were calculated from the propagation of neutron count uncertainty from Desilets (2017). SWE calculated from our lidar observations were biased higher compared to CRNS SWE values with a MBE value of 0.096 cm. The MAE was equal to the MBE between the weighted lidar SWE and CRNS SWE. As seen on Figures 6a and 6b the RMSE was 0.112 and 0.127 cm for each scenario, respectively. Comparing modeled SWE against CRNS SWE showed our model results were slightly biased on average lower compared to CRNS SWE with an MBE = −0.06 cm. The MAE was calculated to be 0.108 cm and the RMSE (Figure 6c) was calculated to be 0.127 cm. The 1:1 line was within estimated uncertainty for nearly every date for all three SWE comparisons.

4. Discussion

4.1. Relationship to Previous Research

Previous studies indicated that a CRNS could detect low amounts of SWE with reasonable uncertainty. Wallbank et al. (2021) used a network of CRNS instruments to record SWE for 254 snow events at 46 sites over five winter seasons. Their instruments were able to detect SWE ranging from 0 to 40 mm, with most of their data reporting below 20 mm, and their CRNS SWE estimates were consistent with the output from the PACK snowmelt model. Sigouin and Si (2016) found that CRNS-estimated SWE between 20 and 60 mm for a Canadian Prairie site agreed with manual SWE surveys with an RMSE of 8.8 mm over the course of two winters. Schattan et al. (2017) used an aboveground CRNS to estimate SWE of deeper snowpacks (values up to 600 mm) in a complex mountainous terrain using TLS and manual snow surveys. Their work found that a CRNS was effective at estimating SWE for an average horizontal footprint of 230 m in the deep snowpack. Jitnikovitch et al. (2021) employed multiple CRNS in the Canadian Arctic and southern Ontario to estimate SWE using linear regression equations. Calibration to manual snow surveys indicated that CRNS are effective at estimating SWE of less than 150 mm. Combined with these previous studies and our work, the CRNS has proven to be effective at estimating SWE for several different environments.

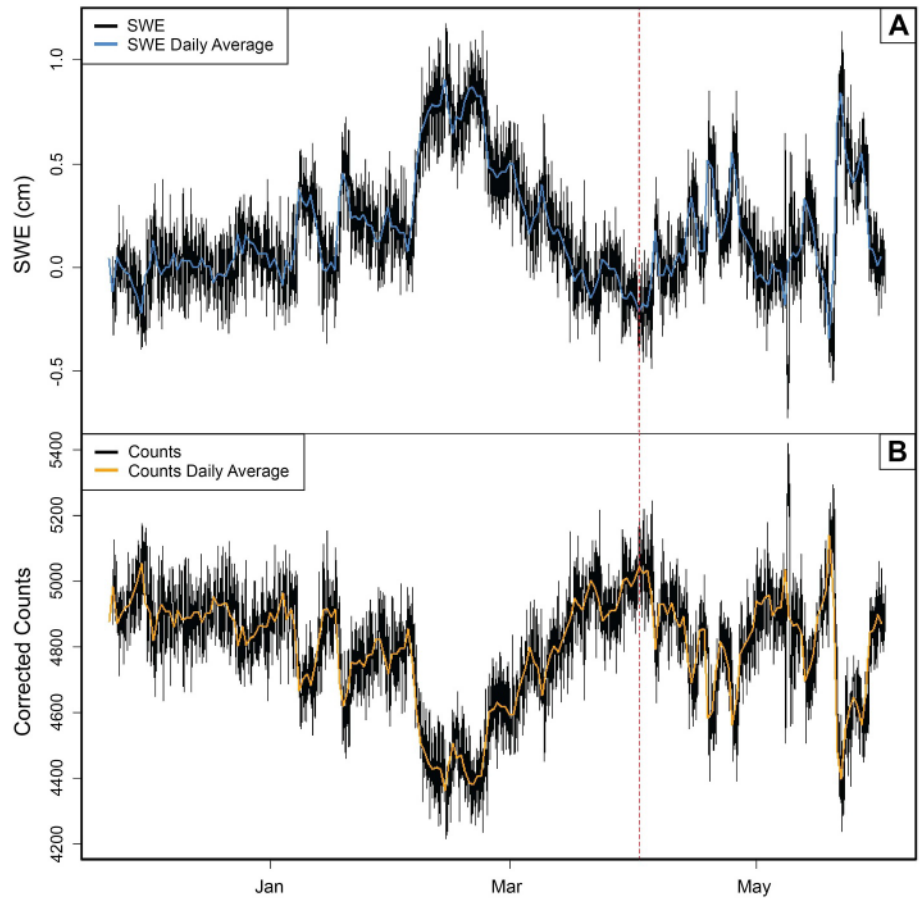


Figure 5. (a) Hourly (black) and daily averaged (blue) snow water equivalent (SWE) estimated from calibrated cosmic ray neutron sensor (CRNS) neutron counts (Desilets, 2017) for the 2020–2021 winter season. (b) Hourly (black) and daily averaged (orange) corrected neutron counts from the moderated channel of the CRNS for the same period. The vertical dashed red line marks 2 April, when the soil moisture and temperature sensors and automated cameras were removed for spring planting of the agricultural fields.

4.2. Considerations for SWE Comparisons

Snow cover at the CARC study site was very shallow and patchy during the study period, based on site observations and UAV lidar data, which is expected for a prairie environment in Montana. Interestingly, in a few cases the CRNS SWE estimates seemed to increase for a short time (hours to days) after snow events occurred. This may be evidence that the sensor detected wind-driven deposition of snow behind the large windbreak within the sensor footprint. A major snowstorm occurred soon before 17 February, and automated camera images showed wind reworking the snow and shifting the position of snow cover, usually resulting in snow drifts increasing in height. Unfortunately, we did not have a shielded precipitation gauge at our site for the 2020–2021 winter that could have provided reliable precipitation data in windy conditions and further confirmed that SWE increases were due to wind redistribution of snowpack within the CRNS footprint. A shielded precipitation gage at the site was installed in 2022, after the conclusion of the study period of this analysis.

We present CRNS SWE data that assumes a constant baseline soil moisture throughout the winter. While soil moisture probes were deployed at the site (Cosh et al., 2022), they could not reliably estimate soil moisture at soil temperatures below approximately 4°C due to the change in dielectric properties during the phase transition between liquid water and ice. The soil temperature remained below 4°C for over 90% of the study period, rendering the soil moisture data largely uninformative. Given that the soil remained frozen for most of the winter, large changes in soil moisture during that time are unlikely. Additionally, the soil moisture measured in early spring from the three soil moisture probe locations within or near the CRNS footprint showed little change

19447973, 2024, 6, Downloaded from https://agupubs.onlinelibrary.wiley.com/doi/10.1029/2024WR037164 by Montana State University Library, Wiley Online Library on [16/08/2024]. See the Terms and Conditions (https://onlinelibrary.wiley.com/terms-and-conditions) on Wiley Online Library for rules of use; OA articles are governed by the applicable Creative Commons License

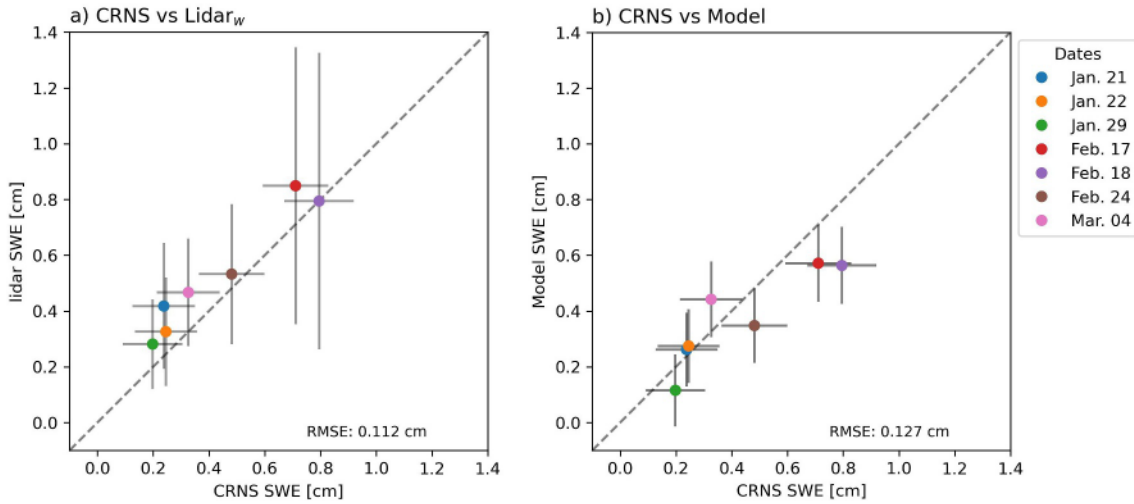


Figure 6. Comparisons between snow water equivalent (SWE) estimates from the CRNS instrument, spatially weighted lidar, and URANOS model simulations. (a) CRNS SWE compared against spatially weighted average lidar-derived SWE. (b) CRNS SWE estimates compared against model simulated SWE. Each plot shows the seven dates of lidar data collection, with RMSEs in the bottom right of each plot and a 1:1 line in black dashes. Estimated uncertainties in each SWE value are shown in black lines.

compared to the late fall. However, continuous, reliable soil moisture observations throughout the winter could provide a more accurate, time-varying soil moisture baseline for estimation of CRNS SWE.

For future work using CRNS instruments in a prairie environment or other windy sites, we recommend pairing CRNS with a shielded precipitation gauge to constrain input of SWE to the environment. This recommendation of a precipitation gauge rather than a snow pillow is due to the significant wind redistribution observed at the site. High winds in the prairie would redistribute snow around the snow pillow, resulting in SWE values that are not necessarily representative of the broader area. Observations with larger spatial coverage, such as CRNS or lidar, allow for more representative snow observations in such conditions. If possible, continuous soil moisture measurements (in non-frozen soils) may help to provide an accurate baseline for estimating SWE.

Multiple sources of uncertainty apply to the lidar-derived SWE estimates that we used to evaluate the CRNS SWE estimates. Palomaki and Sproles (2023) compared snow depth derived from the same lidar data at the CARC for one date, 21 January, to in situ snow depth transect measurements and found lidar RMSE of approximately 20 cm, higher than any RMSEs reported by DJ&A. The ground truth snow depth values used by Palomaki and Sproles (2023) were collected one day before the lidar flight (20 January vs. 21 January, respectively) because the UAV flights were postponed due to high winds. We believe that snow redistribution occurred in the intervening 24 hr, altering snow depths, and leading to increased error. We compared in situ snow depth transect measurements against lidar snow depth data for a second date, 17 February, when the observations were contemporaneous. This yielded an RMSE of 8 cm, which is consistent with the uncertainty of 7.9 cm that DJ&A reported for that date. This led us to trust the uncertainties in DJ&A's analysis and use them in our study. The lidar vertical uncertainties, which include factors such as lidar return noise from crop stubble, lidar instrument positioning, georeferencing lidar returns, aligning lidar point clouds, and identification of the snow and ground surface from point clouds, were about 4–8 cm at our site.

Another source of uncertainty in the lidar-derived SWE results from the shallow snow cover often interspersed with crop stubble. These factors made it difficult to collect snow density measurements over most of the study area, leading to the necessity of relying heavily on limited snow pit data in areas of deep snow for snow density estimates. The two snow pits we used to calculate snow density, Wx and SnowEx1, were located at different ends of the snow drift on the western portion of the site. We assumed snow density measured in different layers within the snow drift was representative across the entire study site for a given lidar collection date, but this assumption comes with some inherent uncertainty that is not readily quantifiable. Future CRNS studies in prairie environments should make every effort to measure the density of shallow snow to reduce this potential source of uncertainty.

19447973, 2024, 6, Downloaded from https://agupubs.onlinelibrary.wiley.com/doi/10.1029/2024WR037164 by Montana State University Library, Wiley Online Library on [16/08/2024]. See the Terms and Conditions (https://onlinelibrary.wiley.com/terms-and-conditions) on Wiley Online Library for rules of use; OA articles are governed by the applicable Creative Commons License

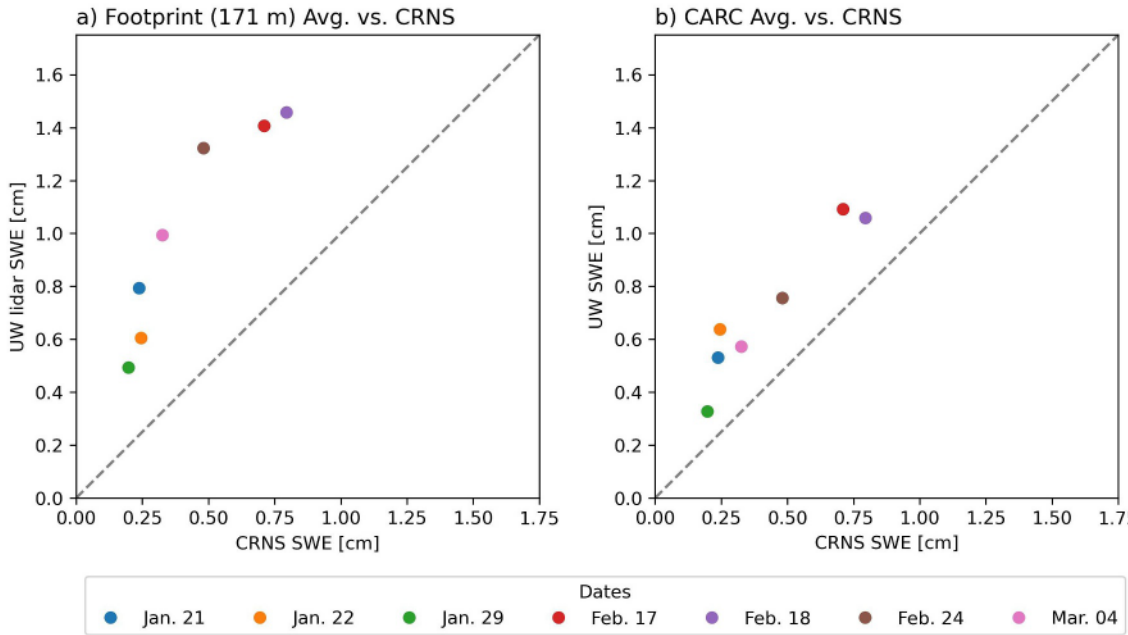


Figure 7. Comparisons between spatially unweighted average lidar snow water equivalent (SWE) and CRNS SWE. (a) Lidar SWE averaged within the 171 m footprint versus CRNS SWE. (b) Lidar SWE averaged for the entire 1 km^2 study domain of the CARC versus CRNS SWE. Each plot shows the seven dates of lidar data collection and a 1:1 line in black dashes.

Our URANOS simulations were also affected by the challenges that arose in obtaining field measurements for this campaign such as the ones described in Section 4.1. The lack of continuous soil moisture verification data at the CARC due to frozen conditions meant we had to rely on soil measurements collected outside of the winter season. As a result, all URANOS simulations mentioned in this study were completed using the same interpolated soil maps of soil moisture, porosity, and bulk density. However, as mentioned in Section 4.1, we expect little change in soil conditions due to the frozen conditions for the entire winter season. The inclusion of soil lattice water also meant that the amount of water stored in the soil was twice the amount of SWE around our CRNS. Obtaining accurate soil water equivalent is a strong factor in obtaining accurate SWE measurements with CRNS in shallow snow environments.

4.3. Spatial Representativeness of CRNS SWE

This study site provides an interesting test bed for evaluating the effect of heterogeneous snow conditions on CRNS observations. Extensive previous literature (Desilets et al., 2010; Schattan et al., 2017, 2019; Schrön et al., 2017; Sigouin & Si, 2016) and our URANOS simulations show that CRNS observations are sensitive to conditions near the sensor, and sensitivity decreases with distance. Overall, our hourly CRNS SWE estimates are low, below 1 cm at all points during the winter. The CARC site experienced a relatively dry winter, which partially accounts for these low CRNS SWE values. However, the low CRNS values also reflect the sensitivity of the CRNS to its surrounding area. The CRNS was in a wheat field often bare of snow due to wind redistribution. Therefore, the CRNS estimates of SWE were lower than the areal average in the surrounding area. This is illustrated in Figure 7, where we compare unweighted areal average lidar-derived SWE to spatially weighted average lidar-derived SWE and to CRNS SWE.

Figure 7 shows that unweighted areal average lidar SWE values are considerably higher compared to CRNS SWE. The unweighted lidar average within the CRNS footprint was biased with a MBE of 0.582 cm compared to CRNS SWE values. However, the agreement is closer to when the unweighted areal average is calculated for the entire 1 km^2 study area. The CARC average SWE were biased higher with a MBE = 0.282 cm compared to CRNS SWE. We attribute these biases to a combination between CRNS spatial sensitivity, representativeness of the CRNS footprint relative to the entire 1 km^2 study area, and bare ground effects. As seen in Figure 4, the footprint of the CRNS intersected with some of the largest snow drifts in the study area, but also very sensitive to the low

19447973, 2024, 6, Downloaded from https://agupubs.onlinelibrary.wiley.com/doi/10.1029/2024WR037164 by Montana State University Library, Wiley Online Library on [16/08/2024]. See the Terms and Conditions (https://onlinelibrary.wiley.com/terms-and-conditions) on Wiley Online Library for rules of use; OA articles are governed by the applicable Creative Commons License

19447973, 2024, 6, Downloaded from https://agupubs.onlinelibrary.wiley.com/doi/10.1029/2024WR037164 by Montana State University Library, Wiley Online Library on [16/08/2024]. See the Terms and Conditions (https://onlinelibrary.wiley.com/terms-and-conditions) on Wiley Online Library for rules of use; OA articles are governed by the applicable Creative Commons License

snow conditions in the area immediately surrounding the CRNS, an often-bare field. These bare fields were more representative of the broader study area that consisted mainly of over-wintering agricultural fields. Because of the increased area of bare fields in the domain of the CARC, the domain average SWE tends to be smaller than the footprint average SWE. In addition, a bare ground tends to bias neutron count rates higher (Schattan et al., 2019).

Overall, these results show that our CRNS measurements are broadly representative of this prairie study site even with heterogeneous snow cover, due to the chosen location of our CRNS. These results both highlight the importance of using an appropriate spatial weighting function when evaluating CRNS SWE in highly heterogeneous conditions, while also emphasizing the importance of siting CRNS in a location that experiences snow conditions that are broadly representative of the area that the user wants to monitor. We plan to further investigate the influence of heterogenous snow cover on CRNS at this prairie site in a future study.

5. Conclusion

This study confronted the CRNS estimates with high resolution distributed snow maps derived from UAV lidar in order to assess whether CRNS can effectively estimate SWE for a prairie site that experiences considerable snowpack spatial heterogeneity. Additionally, we compared CRNS SWE estimates to SWE calculated from URANOS neutron transport model simulations initialized with the UAV-based lidar snow distributions. Our results show that the CRNS is a valuable tool for SWE monitoring in shallow, highly variable prairie snow. The agreement between the CRNS, lidar-derived, and URANOS SWE was about 1–2 mm for the low SWE accumulations observed at the site (about 1 cm or less). The large footprint of CRNS may provide an advantage over conventional SWE observations in highly variable environments such as the prairie, which underscores its potential for ground validation of airborne and satellite snow sensors. Quantifying and calibrating the CRNS sensitivity to both soil moisture and snow in heterogeneous environments are critical steps for analysis. Additionally, given the spatial sensitivity of CRNS, it is important to install the sensor in a location representing the broader area of interest. If the application of a given CRNS is to estimate areal average SWE, then the CRNS should be placed in a location that tends to accumulate an "average" or "characteristic" snowpack for that given area. Future work will use URANOS simulations to further investigate how much snow spatial heterogeneity influences the CRNS SWE signal in shallow, prairie snow environments to best interpret CRNS observations in highly heterogenous environments and provide further recommendations for siting these instruments.

Data Availability Statement

CRNS SWE, lidar, and snow pit data will be uploaded to the NSIDC DAAC and freely available, along with other NASA SnowEx data. Once published, the CRNS SWE data will be available at: https://doi.org/10.5067/NJR0AMMOHZ4E. The snow pit data are freely available from the NSIDC DAAC at: https://doi.org/10.5067/QIANJYJGRWOV. URANOS and CRNS SWE processing code from this analysis is available through GitHub at: https://github.com/heyjoekim/carc_crns and archived on Zenodo at https://doi.org/10.5281/zenodo.11648961.

Acknowledgments
We would like to acknowledge the partial funding we received from the National Aeronautics and Space Administration (NASA) Terrestrial Hydrology Program for their support of this field campaign, including funding the lidar flights, ground-based instruments (aside from the CRNS), and soil calibration sampling. Thank you also to Michael Cosh, USDA ARS, for providing the soil moisture probes used during the SnowEx prairie campaign. We would also like to thank Dr. Eric Sproles' graduate and undergraduate students for their participation in ground-based snow sampling and observation during winter 2020–2021.

References

Andreadis, K. M., Storck, P., & Lettenmaier, D. P. (2009). Modeling snow accumulation and ablation processes in forested environments. *Water Resources Research*, *45*(5), W05429. https://doi.org/10.1029/2008WR007042

Andreasen, M., Jensen, K. H., Bogena, H., Desilets, D., Zreda, M., & Looms, M. C. (2020). Cosmic ray neutron soil moisture estimation using physically based site-specific conversion functions. *Water Resources Research*, *56*(11), e2019WR026588. https://doi.org/10.1029/2019WR026588

Betts, A. K., Desjardins, R., Worth, D., & Cerkowniak, D. (2013). Impact of land use change on the diurnal cycle climate of the Canadian Prairies. *Journal of Geophysical Research: Atmospheres*, *118*(21), 11996–12011. https://doi.org/10.1002/2013JD020717

Brogi, C., Bogena, H. R., Köhli, M., Huisman, J. A., Hendricks Franssen, H.-J., & Dombrowski, O. (2022). Feasibility of irrigation monitoring with cosmic-ray neutron sensors. *Geoscientific Instrumentation, Methods and Data Systems*, *11*(2), 451–469. https://doi.org/10.5194/gi-11-451-2022

Brown, R. D., & Goodison, B. E. (2006). Snow cover. In *Encyclopedia of hydrological sciences*. John Wiley & Sons, Ltd. https://doi.org/10.1002/0470848944.hsa165

Cosh, M. H., Sproles, E. A., Palomaki, R. T., Beck, M., & Mullen, A. (2022). SnowEx21 prairie station in situ dielectric soil moisture and soil temperature Version 1 [Dataset]. *NASA National Snow and Ice Data Center Distributed Active Archive Center*. https://doi.org/10.5067/ZTAP7GH76M9Y

Deems, J. S., Painter, T. H., & Finnegan, D. C. (2013). Lidar measurement of snow depth: A review. *Journal of Glaciology*, *59*(215), 467–479. https://doi.org/10.3189/2013JoG12J154

Desilets, D. (2017). Calibrating a non-invasive cosmic ray soil moisture for snow water equivalent. HydroInnova Technical Document 17-01. https://doi.org/10.5281/ZENODO.439105

Desilets, D., & Zreda, M. (2001). On scaling cosmogenic nuclide production rates for altitude and latitude using cosmic-ray measurements. *Earth and Planetary Science Letters*, *193*(1), 213–225. https://doi.org/10.1016/S0012-821X(01)00477-0

Desilets, D., & Zreda, M. (2013). Footprint diameter for a cosmic-ray soil moisture probe: Theory and Monte Carlo simulations. *Water Resources Research*, *49*(6), 3566–3575. https://doi.org/10.1002/wrcr.20187

Desilets, D., Zreda, M., & Ferré, T. P. A. (2010). Nature's neutron probe: Land surface hydrology at an elusive scale with cosmic rays. *Water Resources Research*, *46*(11), W11505. https://doi.org/10.1029/2009WR008726

Doesken, N. J., & Robinson, D. A. (2009). The challenge of snow measurements. In L. A. Dupigny-Giroux & C. Mock (Eds.), *Historical climate variability and impacts in North America*. Springer. https://doi.org/10.1007/978-90-481-2828-0_15

Dong, J., Ochsner, T. E., Zreda, M., Cosh, M. H., & Zou, C. B. (2014). Calibration and validation of the COSMOS rover for surface soil moisture measurement. *Vadose Zone Journal*, *13*, 4–8. https://doi.org/10.2136/vzj2013.08.0148

Harder, P., Pomeroy, J. W., & Helgason, W. D. (2020). Improving sub-canopy snow depth mapping with unmanned aerial vehicles: Lidar versus structure-from-motion techniques. *The Cryosphere*, *14*(6), 1919–1935. https://doi.org/10.5194/tc-14-1919-2020

Hardy, J. P., Melloh, R., Koenig, G., Marks, D., Winstral, A., Pomeroy, J. W., & Link, T. (2004). Solar radiation transmission through conifer canopies. *Agricultural and Forest Meteorology*, *126*(3), 257–270. https://doi.org/10.1016/j.agrformet.2004.06.012

Hawdon, A., McJannet, D., & Wallace, J. (2014). Calibration and correction procedures for cosmic-ray neutron soil moisture probes located across Australia. *Water Resources Research*, *50*(6), 5029–5043. https://doi.org/10.1002/2013wr015138

He, H., Dyck, M. F., Si, B. C., Zhang, T., Lv, J., & Wang, J. (2015). Soil freezing–thawing characteristics and snowmelt infiltration in Cryalfs of Alberta, Canada. *Geoderma Regional*, *5*, 198–208. https://doi.org/10.1016/j.geodrs.2015.08.001

Jacobs, J. M., Hunsaker, A. G., Sullivan, F. B., Palace, M., Burakowski, E. A., Herrick, C., & Cho, E. (2021). Snow depth mapping with unpiloted aerial system lidar observations: A case study in Durham, New Hampshire, United States. *The Cryosphere*, *15*(3), 1485–1500. https://doi.org/10.5194/tc-15-1485-2021

Jitnikovitch, A., Marsh, P., Walker, B., & Desilets, D. (2021). Snow water equivalent measurement in the Arctic based on cosmic ray neutron attenuation. *The Cryosphere*, *15*(11), 5227–5239. https://doi.org/10.5194/tc-15-5227-2021

Kim, E., Gatebe, C., Hall, D., Newlin, J., Misakonis, A., Elder, K., et al. (2017). NASA's snowEx campaign: Observing seasonal snow in a forested environment. In *2017 IEEE International Geoscience and Remote Sensing Symposium (IGARSS)* (pp. 1388–1390). https://doi.org/10.1109/IGARSS.2017.8127222

Köhli, M., Schrön, M., & Schmidt, U. (2018). Response functions for detectors in cosmic ray neutron sensing. *Nuclear Instruments and Methods in Physics Research Section A: Accelerators, Spectrometers, Detectors and Associated Equipment*, *902*, 184–189. https://doi.org/10.1016/j.nima.2018.06.052

Köhli, M., Schrön, M., Zacharias, S., & Schmidt, U. (2023). URANOS v1.0 – The ultra rapid adaptable neutron-only simulation for environmental research. *Geoscientific Model Development*, *16*(2), 449–477. https://doi.org/10.5194/gmd-16-449-2023

Köhli, M., Schrön, M., Zreda, M., Schmidt, U., Dietrich, P., & Zacharias, S. (2015). Footprint characteristics revised for field-scale soil moisture monitoring with cosmic-ray neutrons. *Water Resources Research*, *51*(7), 5772–5790. https://doi.org/10.1002/2015WR017169

Lehning, M. (2006). Energy balance and thermophysical processes in snowpacks. In *Encyclopedia of hydrological sciences*. John Wiley & Sons, Ltd. https://doi.org/10.1002/0470848944.hsa166

McGrath, D., Webb, R., Shean, D., Bonnell, R., Marshall, H. P., Painter, T. H., et al. (2019). Spatially extensive ground-penetrating radar snow depth observations during NASA's 2017 SnowEx campaign: Comparison with in situ, airborne, and satellite observations. *Water Resources Research*, *55*(11), 10026–10036. https://doi.org/10.1029/2019wr024907

Palomaki, R. T., & Sproles, E. A. (2023). Assessment of L-band InSAR snow estimation techniques over a shallow, heterogeneous prairie snowpack. *Remote Sensing of Environment*, *296*, 113744. https://doi.org/10.1016/j.rse.2023.113744

Pomeroy, J. W., & Li, L. (2000). Prairie and Arctic areal snow cover mass balance using a blowing snow model. *Journal of Geophysical Research*, *105*(D21), 26619–26634. https://doi.org/10.1029/2000JD900149

Rosolem, R., Shuttleworth, W. J., Zreda, M., Franz, T. E., Zeng, X., & Kurc, S. A. (2013). The effect of atmospheric water vapor on neutron count in the cosmic-ray soil moisture observing system. *Journal of Hydrometeorology*, *14*(5), 1659–1671. https://doi.org/10.1175/JHM-D-12-0120.1

Royer, A., Roy, A., Jutras, S., & Langlois, A. (2021). Review article: Performance assessment of radiation-based field sensors for monitoring the water equivalent of snow cover (SWE). *The Cryosphere*, *15*(11), 5079–5098. https://doi.org/10.5194/tc-15-5079-2021

Schattan, P., Baroni, G., Oswald, S. E., Schöber, J., Fey, C., Kormann, C., et al. (2017). Continuous monitoring of snowpack dynamics in alpine terrain by aboveground neutron sensing. *Water Resources Research*, *53*(5), 3615–3634. https://doi.org/10.1002/2016WR020234

Schattan, P., Köhli, M., Schrön, M., Baroni, G., & Oswald, S. E. (2019). Sensing area-average snow water equivalent with cosmic-ray neutrons: The influence of fractional snow cover. *Water Resources Research*, *55*(12), 10796–10812. https://doi.org/10.1029/2019WR025647

Schrön, M., Köhli, M., Scheiffele, L., Iwema, J., Bogena, H. R., Lv, L., et al. (2017). Improving calibration and validation of cosmic-ray neutron sensors in the light of spatial sensitivity. *Hydrology and Earth System Sciences*, *21*(10), 5009–5030. https://doi.org/10.5194/hess-21-5009-2017

Schrön, M., Zacharias, S., Womack, G., Köhli, M., Desilets, D., Oswald, S. E., et al. (2018). Intercomparison of cosmic-ray neutron sensors and water balance monitoring in an urban environment. *Geoscientific Instrumentation, Methods and Data Systems*, *7*(1), 83–99. https://doi.org/10.5194/gi-7-83-2018

Serreze, M. C., Clark, M. P., Armstrong, R. L., McGinnis, D. A., & Pulwarty, R. S. (1999). Characteristics of the western United States snowpack from snowpack telemetry (SNOTEL) data. *Water Resources Research*, *35*(7), 2145–2160. https://doi.org/10.1029/1999WR900090

Shook, K., & Gray, D. M. (1994). Determining the snow water equivalent of shallow prairie snowcovers. In *Proceedings of the 51st Eastern Snow Conference, Dearborn, Michigan, USA* (pp. 89–95).

Shook, K., & Gray, D. M. (1997). Synthesizing shallow seasonal snow covers. *Water Resources Research*, *33*(3), 419–426. https://doi.org/10.1029/96WR03532

Sigouin, M. J. P., & Si, B. C. (2016). Calibration of a non-invasive cosmic-ray probe for wide area snow water equivalent measurement. *The Cryosphere*, *10*(3), 1181–1190. https://doi.org/10.5194/tc-10-1181-2016

Sturm, M., Goldstein, M. A., & Parr, C. (2017). Water and life from snow: A trillion-dollar science question. *Water Resources Research*, *53*(5), 3534–3544. https://doi.org/10.1002/2017WR020840

Sturm, M., Holmgren, J., & Liston, G. E. (1995). A seasonal snow cover classification system for local to global applications. *Journal of Climate*, *8*(5), 1261–1283. https://doi.org/10.1175/1520-0442(1995)008<1261:ASSCCS>2.0.CO;2

Todhunter, P. E. (2001). A hydroclimatological analysis of the Red River of the North snowmelt flood catastrophe of 1997. *Journal of the American Water Resources Association*, *37*(5), 1263–1278. https://doi.org/10.1111/j.1752-1688.2001.tb03637.x

19447973, 2024, 6, Downloaded from https://agupubs.onlinelibrary.wiley.com/doi/10.1029/2024WR037164 by Montana State University Library, Wiley Online Library on [16/08/2024]. See the Terms and Conditions (https://onlinelibrary.wiley.com/terms-and-conditions) on Wiley Online Library for rules of use; OA articles are governed by the applicable Creative Commons License

USDA, N. M. F. O. (2022). USDA/NASS 2021 state agriculture overview for Montana. 2021 State Agriculture Overview - Montana. Retrieved from https://www.nass.usda.gov/Quick_Stats/Ag_Overview/stateOverview.php?state=MONTANA

Wallbank, J. R., Cole, S. J., Moore, R. J., Anderson, S. R., & Mellor, E. J. (2021). Estimating snow water equivalent using cosmic-ray neutron sensors from the COSMOS-UK network. *Hydrological Processes*, *35*(5), e14048. https://doi.org/10.1002/hyp.14048

Zreda, M., Desilets, D., Ferré, T. P. A., & Scott, R. L. (2008). Measuring soil moisture content non-invasively at intermediate spatial scale using cosmic-ray neutrons. *Geophysical Research Letters*, *35*(21), L21402. https://doi.org/10.1029/2008GL035655

Zreda, M., Shuttleworth, W. J., Zeng, X., Zweck, C., Desilets, D., Franz, T., & Rosolem, R. (2012). COSMOS: The COsmic-ray Soil Moisture Observing System. *Hydrology and Earth System Sciences*, *16*(11), 4079–4099. https://doi.org/10.5194/hess-16-4079-2012

19447973, 2024, 6, Downloaded from https://agupubs.onlinelibrary.wiley.com/doi/10.1029/2024WR037164 by Montana State University Library, Wiley Online Library on [16/08/2024]. See the Terms and Conditions (https://onlinelibrary.wiley.com/terms-and-conditions) on Wiley Online Library for rules of use; OA articles are governed by the applicable Creative Commons License